Si clusters are more metallic than bulk Si

Koblar Jackson and Julius Jellinek

Citation: J. Chem. Phys. **145**, 244302 (2016); doi: 10.1063/1.4972813
View online: http://dx.doi.org/10.1063/1.4972813
View Table of Contents: http://aip.scitation.org/toc/jcp/145/24
Published by the American Institute of Physics

Si clusters are more metallic than bulk Si

Koblar Jackson[1,a)] and Julius Jellinek[2,a)]
[1]*Physics Department and Science of Advanced Materials Program, Central Michigan University, Mount Pleasant, Michigan 48859, USA*
[2]*Chemical Sciences and Engineering Division, Argonne National Laboratory, Argonne, Illinois 60439, USA*

(Received 15 October 2016; accepted 8 December 2016; published online 22 December 2016)

Dipole polarizabilities were computed using density functional theory for silicon clusters over a broad range of sizes up to $N = 147$ atoms. The calculated total effective polarizabilities, which include contributions from permanent dipole moments of the clusters, are in very good agreement with recently measured values. We show that the permanent dipole contributions are most important for clusters in the intermediate size range and that the measured polarizabilities can be used to distinguish between energetically nearly degenerate cluster isomers at these sizes. We decompose the computed total polarizabilities α into the so-called dipole and charge transfer contributions, α^p and α^q, using a site-specific analysis. When the per-atom values of these quantities are plotted against $N^{-1/3}$, clear linear trends emerge that can be extrapolated to the large size limit ($N^{-1/3} \rightarrow 0$), resulting in a value for $\frac{\alpha}{N}$ of 30.5 bohrs^3/atom that is significantly larger than the per-atom polarizability of semiconducting bulk Si, 25.04 bohrs^3/atom. This indicates that Si clusters possess a higher degree of metallicity than bulk Si, a conclusion that is consistent with the strong electrostatic screening of the cluster interiors made evident by the analysis of the calculated atomic polarizabilities. *Published by AIP Publishing.* [http://dx.doi.org/10.1063/1.4972813]

I. INTRODUCTION

Silicon clusters (Si_N) have been studied for nearly three decades, reflecting not only the fundamental interest in how silicon, the prototypical semiconductor, behaves in the range of small sizes but also the fascinating and peculiar properties of the clusters themselves. For example, early experimental studies of Si_N using time-of-flight mass spectrometry indicated a remarkable transition in the shapes of Si_N over the size range $N = 16$–30.[1] The most stable structures of the clusters grow increasingly prolate with size up to around $N = 26$, beyond which compact structures are preferred. The discovery of this shape transition generated a wave of theoretical work seeking to determine the most stable atomic arrangements of Si_N.[2–10] Extensive structural searches based on density functional theory (DFT)[4,6,9] yielded lowest-energy isomers across the shape transition size range ($N = 16$–26) which were consistent with experimental ion mobility data[11] and measured cluster dissociation energies.[12] More recent calculations have focused on cluster sizes beyond N = 26.[13–26] Stuffed-fullerene structures,[13] which can be thought of as fullerene-like shells encapsulating smaller groups of interior atoms, have the lowest-energies reported yet for sizes up to N = 80.[17,18,20,22]

The dipole polarizability describes the response of a system to an external electric field. Since the concept of material type, i.e., insulator, semiconductor, or metal, is not well defined for clusters, the polarizability is a useful quantity that allows for a direct comparison of the type of response of cluster matter to that of the corresponding bulk material. Silicon cluster polarizabilities have been studied both experimentally and theoretically. Early calculations[27–31] found that small clusters are more polarizable on a per-atom basis than crystalline silicon (c-Si). Computational studies also indicated that the total cluster polarizability strongly depends on the cluster shape: prolate clusters have significantly larger polarizabilities than the more compact spherical or near-spherical forms at the same cluster size.[32,33] Early experimental data[34] turned out to be at odds with the results of the computations and pointed to cluster polarizabilities smaller than that of c-Si.[34] More accurate polarizability measurements were performed recently for clusters in the size range $N = 8$–75.[35,36] The new experimental data reversed the earlier measured findings, indicating that the polarizabilities of Si_N approach the bulk limit from above. These data also showed that the permanent cluster dipole moments have a strong effect on the measured polarizabilities, particularly in the size-range of the shape transition.

The new experimental results motivated us to perform new DFT calculations of Si_N polarizabilities over a size range that includes and exceeds that covered by the experiments. Our goal is twofold: (1) to establish the extent to which the computations systematically reproduce the measured polarizabilities and (2) to provide deeper insights into the nature of the polarizability response in Si_N. To accomplish this, we use our site-specific methodology[33,37] that provides for a decomposition of the total cluster polarizability α into atomic contributions α^A, as well as its dipole, α^p, and charge transfer, α^q, components. While the metallic-like behavior of small Si clusters was addressed in an earlier paper,[32] here we show that this behavior persists to much larger sizes. The extended size range covered in this study allows for establishing clear trends in the size-evolution

a)Authors to whom correspondence should be addressed. Electronic addresses: jacks1ka@cmich.edu, Telephone: 989-774-3310 and jellinek@anl.gov, Telephone: 630-252-3463.

of $\frac{\alpha^p}{N}$ and $\frac{\alpha^q}{N}$. These trends are difficult to discern directly from the size-evolution of $\frac{\alpha}{N}$, so the methodology of site-specific polarizabilities we use here—including the decomposition into the dipole and charge-transfer components—is essential for the analysis presented below. Specifically we show that, on one hand, the polarizabilities calculated for the extended size range are in good agreement with the results of the recent measurements. On the other hand, the size-dependent trends in $\frac{\alpha^p}{N}$ and $\frac{\alpha^q}{N}$ over this size range, when extrapolated to the macroscopic limit, converge to values that when added together are more than 20% larger than the polarizability per atom of bulk silicon (c-Si). This is consistent with the strong, metallic-like electrostatic screening of the Si cluster interiors from an external electric field that is evident in the site-specific (atomic) polarizabilities. We discuss the changes in the size-dependent trends in $\frac{\alpha^p}{N}$ and $\frac{\alpha^q}{N}$ that will have to take place at larger sizes to obtain the correct value of the polarizability of c-Si.

II. METHODOLOGY

The DFT calculations were carried out using the generalized gradient approximation of Perdew, Burke, and Enzerhof (DFT-PBE)[38] as implemented in the NRLMOL code.[39,40] NRLMOL employs extensive Gaussian-orbital basis sets that are optimized for use with the PBE functional.[41] The Si basis consists of 6 s-type, 5 p-type, and 4 d-type orbitals for each Si atom, with a longest-ranged Gaussian exponent of 0.053 956. The DFT-PBE-NRLMOL computational approach has been shown to give a good description of Si clusters.[9]

The site-specific partitioning scheme described in detail in Ref. 33 was used to analyze the polarizabilities. As a brief recap, we recall that the total cluster polarizability can be expressed as the zero-field derivative of the cluster electric dipole moment $\vec{\mu}$ with respect to a uniform external electric field, $\vec{E}$,

$$\alpha_{ij} = \left.\frac{d\mu_i}{dE_j}\right|_{E=0}, \tag{1}$$

where i and j label the x, y, and z components of $\vec{\mu}$ and $\vec{E}$, respectively. $\vec{\mu}$ can be written as an integral over the total (including nuclear charges) charge density, $\rho(\vec{r})$, and decomposed into constituent atomic dipole moments $\vec{\mu}^A$ via a Voronoi partitioning of space into non-overlapping atomic volumes Ω_A. The partitioning is easily and accurately realized using the numerical integration grid in NRLMOL.[39] The $\vec{\mu}^A$ can then be expressed as[33]

$$\vec{\mu}^A = \int_{\Omega_A} \rho(\vec{r})\left(\vec{r} - \vec{R}_A\right) d\vec{r} + q_A\vec{R}_A, \tag{2}$$

where $\vec{R}_A$ is the position of the nucleus of atom A and q_A is the net charge inside the volume Ω_A associated with it. The terms on the right hand side of Eq. (2) are, respectively, the dipole $\vec{\mu}^{A,p}$ and charge-transfer $\vec{\mu}^{A,q}$ components of $\vec{\mu}^A$. $\vec{\mu}^{A,p}$ is the local dipole moment due to the distribution of the electron charge density inside Ω_A relative to $\vec{R}_A$, whereas $\vec{\mu}^{A,q}$ is the dipole moment of a point charge of magnitude q_A located at $\vec{R}_A$ with respect to the origin of the coordinate system. The derivatives of $\vec{\mu}^{A,p}$ and $\vec{\mu}^{A,q}$ with respect to the external electric field $\vec{E}$ are, respectively, the dipole $\alpha_{ij}^{A,p}$ and charge-transfer $\alpha_{ij}^{A,q}$ components of the site (or atomic) polarizabilities $\alpha_{ij}^A \left(= d\mu_i^A/dE_j\right)$. A benefit of decomposing α_{ij}^A into $\alpha_{ij}^{A,p}$ and $\alpha_{ij}^{A,q}$ is that $\alpha_{ij}^{A,p}$ reflects the field-induced redistribution of the electron charge density within the volume Ω_A and serves as a measure of a dielectric-type of response, whereas $\alpha_{ij}^{A,q}$ reflects the change in the charge q_A of volume Ω_A (the field may cause electron charge transfer from one atomic volume to another) and serves as a measure of a metallic-type of response.[33] The sums of $\alpha_{ij}^{A,p}$ and $\alpha_{ij}^{A,q}$ over all atoms constitute the dipole and charge-transfer components of the total cluster polarizability ($\alpha_{ij} = \alpha_{ij}^p + \alpha_{ij}^q$).

Because the value of $\vec{R}_A$ depends on the choice of the origin of the system of coordinates, so does the value of $\vec{\mu}^{A,q}$, unless $q^A = 0$, whereas the value of $\vec{\mu}^{A,p}$ does not depend on this choice. The origin-dependence of $\vec{\mu}^{A,q}$ is a reflection of the well-known fact that the value of the dipole moment of a charge distribution with a non-zero net charge is origin-dependent. As a consequence, $\alpha_{ij}^{A,q}$ (but not $\alpha_{ij}^{A,p}$) also depends on the choice of the origin of the system of coordinates, albeit only when the atomic charge q^A changes with the applied external field (i.e., when $\frac{dq^A}{dE_j} \neq 0$). The total atomic polarizability α_{ij}^A is then, in general, also origin-dependent. For the consistency of comparison of the values of α_{ij}^A within a cluster, between different forms of a cluster, and between clusters of different sizes, we place the origin of the coordinate system at the center of mass of each cluster.

One should note that even though the values of the individual atomic polarizabilities α_{ij}^A depend on the choice of the origin of the coordinate system, the value of the total cluster polarizability α_{ij} does not depend on this choice, and that holds irrespective of whether the cluster is charged or not (the underlying reason is that the total cluster charge does not change when an external field is applied). Since the atomic $\alpha_{ij}^{A,p}$ are origin-independent, the total cluster dipole polarizability α_{ij}^p is origin-independent as well. The origin-independence of α_{ij} and α_{ij}^p then implies that the total cluster charge-transfer polarizability α_{ij}^q is also origin-independent. Hence, all three total cluster descriptors, α_{ij}, α_{ij}^p, and α_{ij}^q, are well-defined and have unique values (see also Ref. 33).

The derivatives involved in the computation of the polarizabilities were obtained using the finite difference method with a field strength of 0.001 a.u. Tests indicate that this choice converges the calculated polarizabilities to better than 0.5%. The results presented below are analyzed in terms of isotropic averages $\alpha = \frac{1}{3}\sum_{i=1}^{3}\alpha_{ii}$ of the polarizabilities.

The calculations were performed for a broad range of Si_N. For clusters of small and medium sizes ($N \leq 28$), we used the most stable isomers obtained earlier via extensive computational searches.[3,4,6,9] For N = 30, 35, 40, 45, 50, 55, 60, 70, 80, and 147, atomic coordinates for multiple candidate structures at each size were obtained from the Cambridge Cluster Database[42] and other sources. These structures were found in constrained searches that in most cases assumed the stuffed-fullerene motif.[16–18,20,22] All the structures were reoptimized without symmetry constraints using DFT-PBE and NRLMOL.

In a number of cases the geometry optimization was followed by normal mode analysis to confirm that the resulting structure corresponds to a minimum of the potential energy surface. The polarizabilities presented below generally refer to the lowest-energy isomer found for each cluster size. For a few select sizes, polarizabilities of higher energy isomers are presented as well for comparison with experimental data. A detailed comparative analysis of the polarizabilities of various isomers at each cluster size will be given elsewhere.

III. RESULTS

A selection of low-energy structures of Si_N at a few representative sizes is shown in Fig. 1. In the smallest size range ($N < 10$), the clusters transition from planar to three-dimensional geometries and contain only surface atoms. In the size range N = 16-25, they become increasingly prolate, but at N = 26 a prolate and a compact conformation are essentially degenerate.[9] In the prolate structures all atoms are on the surface, whereas in the compact, more spherical conformations, a small number of atoms are in the interior. The lowest-energy isomers beyond N = 30 all have stuffed-fullerene structures.

Table I shows the calculated values of $\frac{\alpha}{N}$, $\frac{\alpha^p}{N}$, and the magnitude of the permanent (i.e., zero-field) dipole moment $\mu = |\vec{\mu}|$ for Si_N as a function of N. The values of $\frac{\alpha^p}{N}$ steadily decrease with increasing cluster size, and at all sizes and for all isomers, there is a sizable dipole moment. $\frac{\alpha^q}{N}$ provides a larger contribution to $\frac{\alpha}{N}$ than $\frac{\alpha^p}{N}$ at all sizes shown in the table.

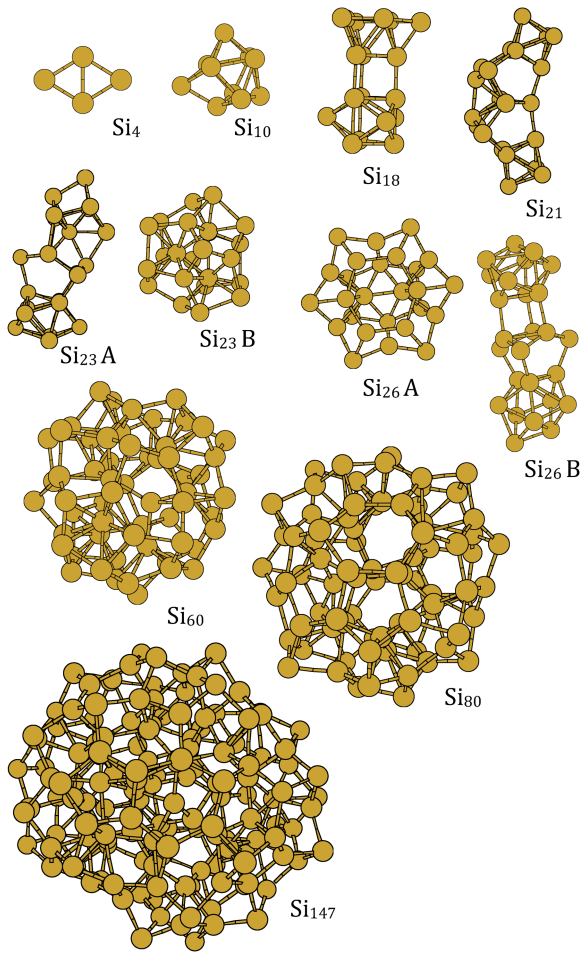

FIG. 1. A representative selection of the silicon cluster structures used in this study. The labels indicate the cluster sizes. Multiple isomers are labeled as A and B in the order of increasing energy (decreasing stability). Similar labeling is used in Table I.

TABLE I. Computed values of the per atom total polarizability $\frac{\alpha}{N}$, local dipole polarizability $\frac{\alpha^p}{N}$, dipole moment μ, and effective per atom polarizability $\frac{\alpha^{eff}}{N}$ for Si_N clusters over a range of sizes N. The corresponding experimental per atom polarizabilities $\frac{\alpha^{expt}}{N}$ from Ref. 36 are also listed along with their uncertainties. The labels A and B correspond to the lowest and next lowest energy isomers, respectively.

N	α^{tot} (bohrs^3/atom)	α^p (bohrs^3/atom)	μ (a.u.)	α^{eff} (bohrs^3/atom)	α^{expt} (bohrs^3/atom)
18	33.06	11.08	1.63	84.69	83.50 ± 16
21	34.41	10.71	0.56	39.63	38.74 ± 18
23A	33.76	10.68	1.13	53.11	30.16
23B	30.42	9.93	0.32	31.98	30.16
26A	31.73	9.49	0.53	35.50	53.75 ± 16
26B	34.23	10.47	1.04	48.69	53.75 ± 16
30	31.24	9.23	0.23	31.87	29.61 ± 5.7
35	30.49	8.57	0.55	33.48	27.47 ± 4.4
40	30.35	8.15	0.44	32.06	23.99 ± 12
45	29.81	7.75	0.96	37.03	31.40 ± 4.1
50	30.41	7.53	0.51	32.21	29.59 ± 4.0
55	30.66	7.31	0.60	32.95	30.99 ± 5.0
60	30.10	7.13	0.38	30.93	27.81 ± 13
70	30.69	6.90	1.17	37.52	21.71 ± 15.8
80	30.61	6.62	0.90	34.16	...
147	30.56	5.42	1.23	34.20	...

For clusters with a permanent dipole moment, the measured polarizability is different from the isotropically averaged polarizability α because of the tendency of the dipole moment to align with the external electric field. The degree of alignment depends on the temperature as it gets reduced by thermal fluctuations of the direction of the dipole moment: the higher the temperature, the lower the degree of alignment. For comparison with experimental data measured at finite temperatures, the calculated isotropically averaged polarizability α therefore has to be converted into a temperature-dependent effective polarizability α^{eff},

$$\frac{\alpha^{eff}}{N} = \frac{\alpha}{N} + \frac{\mu^2}{3NkT}. \tag{3}$$

The experiments[36] were performed at room temperature and we use T = 300 K to obtain α^{eff} from α and μ. The values of $\frac{\alpha^{eff}}{N}$ together with those of $\frac{\alpha^{expt}}{N}$ and its uncertainty are also listed in Table I.

Inspection of the table indicates very good agreement between the calculated $\frac{\alpha^{eff}}{N}$ and measured $\frac{\alpha^{expt}}{N}$ values. The DFT-PBE results reproduce the experimental values within the error bars for nearly every size. At a few select sizes, the comparison between the calculated and measured data is particularly noteworthy. For example, the agreement at N = 18 is excellent and is typical of the level of agreement at neighboring sizes. The dipole contribution to $\frac{\alpha^{eff}}{N}$ for Si_{18} is very large, due to the large value of μ, which lies essentially along the prolate axis of the structure as shown in Fig. 1. The agreement at N = 21 is also very good, but in this case the dipole

contribution is much smaller. As can be seen in Fig. 1, Si_{21} is even more prolate than Si_{18}, but its dipole moment is much smaller because of the symmetry in the prolate direction. At $N = 23$ and 26, the value of $\frac{\alpha^{eff}}{N}$ for the lowest-energy isomer does not match with that of $\frac{\alpha^{expt}}{N}$. At $N = 23$, $\frac{\alpha^{eff}}{N}$ clearly includes a large dipole contribution, whereas $\frac{\alpha^{expt}}{N}$ apparently does not; at N = 26, the situation is exactly reversed. At these latter two sizes, a second low-energy isomer exists for which the computed $\frac{\alpha^{eff}}{N}$ agrees with the measured $\frac{\alpha^{expt}}{N}$. At $N = 23$, the compact isomer 23B (see Fig. 1) is only 0.26 eV higher in energy than the prolate structure 23A, and the value of its $\frac{\alpha^{eff}}{N}$ = 31.98 bohrs^3/atom is in excellent agreement with the corresponding value of $\frac{\alpha^{expt}}{N}$ = 30.16 bohrs^3/atom. Similarly, the prolate isomer 26B (see Fig. 1) is only 0.03 eV higher in energy than the compact conformation 26A, and its $\frac{\alpha^{eff}}{N}$ = 48.90 bohrs^3/atom compares well with the corresponding $\frac{\alpha^{expt}}{N}$ = 53.75 bohrs^3/atom. These results suggest that the comparison of the $\frac{\alpha^{eff}}{N}$ and $\frac{\alpha^{expt}}{N}$ values can serve in the intermediate size range as an indicator of the isomer(s) of Si_N actually generated in an experiment. This is important because the DFT approach cannot be expected to always give the correct energy ordering of nearly degenerate isomers. On the other hand, the overall close agreement between theory and experiment seen in Table I shows that DFT-PBE faithfully describes the interaction of silicon clusters with an external electric field.

The dipole moment contribution to $\frac{\alpha^{eff}}{N}$ for N ≥ 30 is seen in Table I to be much smaller than it is over the shape transition size range. The magnitude of μ is generally not smaller for the larger clusters, but the 1/N factor in Eq. (3) reduces the relative size of the dipole term. An interesting implication of this is that the measured $\frac{\alpha^{expt}}{N}$ may not, in general, be as informative for distinguishing between competing isomers at larger sizes as it is at smaller sizes. As the importance of dipole-related differences is diminished with increasing cluster size, isomers would have to be distinguished on the basis of differences in $\frac{\alpha}{N}$. But the experimental uncertainties in $\frac{\alpha^{expt}}{N}$ are typically much larger than differences in $\frac{\alpha}{N}$ for competing isomers, even when the isomers are very different structurally. The data in Table I for isomers 26A and 26B provide a good example to illustrate this point. The computed values of $\frac{\alpha}{N}$ for 26A and 26B differ by only 2.43 bohrs^3/atom, despite their radically different structures (see Fig. 1). For most isomers with $N \geq 30$, the difference is smaller. By contrast, the smallest uncertainty in $\frac{\alpha^{expt}}{N}$ reported for $N \geq 30$ is much larger, ±4 bohrs^3/atom. Despite the relatively large experimental uncertainties, the overall agreement between $\frac{\alpha^{eff}}{N}$ and $\frac{\alpha^{expt}}{N}$ for the larger sizes (see Table I) does show that the stuffed-fullerene structures possess polarizabilities that are generally consistent with those observed in the experiments.

What can the calculated polarizabilities reveal about the nature of the response of Si clusters to an external electric field? To answer this question, we examine the local dipole and charge transfer components of the total cluster polarizabilities. Figure 2 shows the values of $\frac{\alpha}{N}$, $\frac{\alpha^p}{N}$, and $\frac{\alpha^q}{N}$ plotted versus $N^{-1/3}$. Neglecting sizes smaller than $N = 6$ ($N^{-1/3} > 0.58$), for which the clusters have planar structures, clear linear trends can be seen for $\frac{\alpha^p}{N}$ and $\frac{\alpha^q}{N}$. Over the size range N = 15-26 ($N^{-1/3}$ = 0.33-0.40), the $\frac{\alpha^q}{N}$ values deviate from the strict linear trend. The comparatively large values of the polarizabilities in this size range are caused by the strongly prolate shape of the preferred structures. As discussed elsewhere,[33,37] shape-related fluctuations in $\frac{\alpha}{N}$ derive almost entirely from the $\frac{\alpha^q}{N}$ contribution. In Fig. 2, $\frac{\alpha^p}{N}$ shows only minor deviations from the linear trend over the range at hand. As further evidence for the fact that the deviations from linearity in $\frac{\alpha^q}{N}$ are indeed related to the cluster shape, the value of $\frac{\alpha^q}{N}$ for the compact isomer of $N = 23$ ($N^{-1/3} = 0.35$) is also shown in the figure as an open circle. The circle falls on the trend line, demonstrating that the linear dependence on $N^{-1/3}$ reflects size-driven changes in $\frac{\alpha^q}{N}$ when shape-related effects are removed.

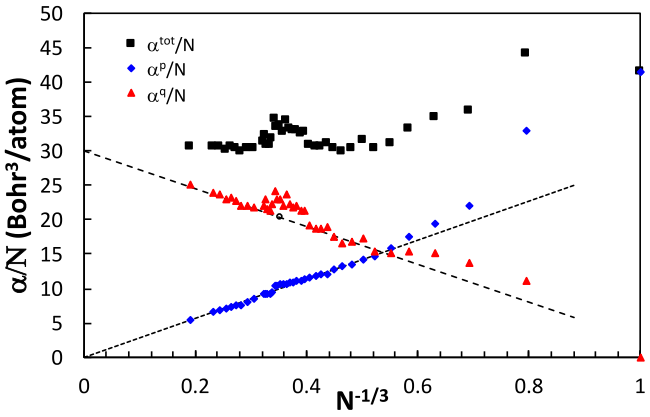

FIG. 2. The computed per atom values of the total cluster polarizability $\frac{\alpha}{N}$ (squares) and its local dipole $\frac{\alpha^p}{N}$ (diamonds) and charge transfer $\frac{\alpha^q}{N}$ (triangles) components plotted vs $N^{-1/3}$. The dotted lines are included as guides to the eye. The open circle at $N^{-1/3} = 0.35$ is the value of $\frac{\alpha^q}{N}$ for the compact isomer 23B.

The trend lines in Fig. 2 are easily extrapolated to the large size limit, giving a value very close to zero for $\frac{\alpha^p}{N}$ and approximately 30.5 bohrs^3/atom for $\frac{\alpha^q}{N}$. Since $\frac{\alpha}{N}$ is the sum of $\frac{\alpha^p}{N}$ and $\frac{\alpha^q}{N}$, its limiting value is also 30.5 bohrs^3/atom.

The polarizability per atom of a bulk material with dielectric constant ϵ can be obtained using the Clausius-Mossotti relation,

$$\frac{\alpha}{N} = \frac{3}{4\pi}\left(\frac{\epsilon - 1}{\epsilon + 2}\right) V_0, \tag{4}$$

where V_0 is the volume per atom of the material. Using the mass density 2330 kg/m^3 of c-Si, its dielectric constant ϵ = 11.7, and the atomic weight 28.05 of the Si atom, one obtains from Eq. (4) the value of $\frac{\alpha^{c-Si}}{N}$ = 25.0 bohrs^3/atom for c-Si. Direct DFT calculations[43] for the dielectric constant of c-Si give ϵ = 12.4, which leads to $\frac{\alpha}{N}$ = 25.4 bohrs^3/atom. These results together with the good agreement between the calculated and measured data in Table I indicate that DFT properly describes the polarizability response of Si at both the bulk limit and in the cluster size regime.

In the limit $\epsilon \to \infty$, Eq. (4) gives the polarizability per atom of a bulk metal. As a gedanken experiment, we use the volume per atom of c-Si in Eq. (4) and assume that it is a metal, obtaining the value of $\frac{\alpha}{N}$ = 32.1 bohrs^3/atom. It is close to the limit value of 30.5 bohrs^3/atom derived from the linear trends exhibited in Fig. 2. The overall conclusion from the

preceding considerations is that, as judged by the large-size limit value of polarizability derived from the size-dependence of the cluster polarizability over the size range covered in this study, Si clusters exhibit a higher degree of metallicity than c-Si, which is a semiconductor with a finite ϵ.

This conclusion finds further corroboration through the analysis of electrostatic screening of the cluster interiors. Large values of $\alpha^{A,p}$ and $\alpha^{A,q}$ reflect significant changes in the electron density around a given interior site (atom) in response to an external electric field and indicate weak screening. Conversely, small values of $\alpha^{A,p}$ and $\alpha^{A,q}$ imply little or no change in the site (atomic) charge density and indicate strong screening. In Fig. 3 we show the value of $\alpha^A = \alpha^{A,p} + \alpha^{A,q}$ for all atoms in Si_{80} versus R_A, the distance of atom A from the cluster center of mass. α^A is essentially zero for the atoms that are the closest to the center of mass, which points to a substantial screening of the cluster interior, and it gradually increases in magnitude as the location of the atoms gets closer to the cluster surface. The increase in α^A from zero to its maximum value occurs over a range of R_A that is about 2.5 Å in extent. We find approximately the same screening thickness for all cluster sizes considered here, and it is close to the bond length in c-Si, 2.35 Å.

It is of interest to consider the physical origins of the linear trends in Fig. 2. From Fig. 3 it is clear that the contributions to α^p are coming mainly from the atoms near the surface. Since the number of these atoms is of the order $N^{2/3}$, the total α^p scales as $N^{2/3}$, and $\frac{\alpha^p}{N}$ can therefore be expected to scale as $N^{-1/3}$.[33] This is exactly the behavior seen in Fig. 2. For α^q it is more convenient to think in terms of an effective radius R of a cluster. The individual contributions to α^q again come from atoms near the cluster surface, and there are order R^2 of these atoms. But since the charge transfer components of the dipole moments of these atoms—and consequently of their polarizabilities (see Eq. (2) and Ref. 33)—already contain a factor of R, the total α^q should scale as R^3. Stated differently, $(\alpha^q)^{\frac{1}{3}}$ should behave like an effective cluster radius, i.e., $R_{eff} = (\alpha^q)^{\frac{1}{3}}$. While defining a precise geometrical radius of a cluster is problematic, it is reasonable to expect that its size is well reflected by a quantity that we call R_{max} and define as the average value of R_A for the four outermost atoms in the cluster. We choose four atoms for this definition in order to smooth out the variations that can occur in specific cluster geometries and because the four outermost atoms tend to lie in different directions from the cluster center, giving a better measure of its overall size. The standard deviation of the four R_A values from R_{max} is a convenient measure of the spread in these values, and it can serve as a measure of the uncertainty in the definition of R_{max}. In Fig. 4 we plot the value of R_{eff} and R_{max} vs the cluster size N for $N \geq 30$. The standard deviations for the R_{max} values are shown as vertical error bars. It can be seen that R_{eff} and R_{max} are close and grow together as N increases. The increase of $\frac{\alpha^q}{N}$ with N (or with decrease of $N^{-1/3}$ as shown in Fig. 2) therefore implies an increase in the volume per atom of the cluster as N increases. What accounts for this change in the volume? The atoms near the center of the stuffed fullerene clusters are arranged in a way that is similar to the open, diamond-like structure of c-Si. The atoms near the surface, by contrast, prefer close-packed arrangements in order to minimize the number of dangling bonds that would otherwise exist on the cluster surface. Since the close-packed arrangements leave less volume for each atom, the entire cluster occupies less volume per atom than the same number of atoms in c-Si. With increasing N, the fraction of the interior atoms increases, and therefore the volume per atom in Si_N increases as well.

In Fig. 5 we present, as a complementary characteristic, the HOMO-LUMO gap of the clusters as a function of their size. For each size, the gap shown is that of the most stable cluster structure. The HOMO-LUMO gap displays oscillatory behavior at small sizes with an overall decrease in magnitude, which is similar to that exhibited by clusters of metallic elements (cf., e.g., Refs. 44 and 45). This, together with the fact that at larger sizes (N ≥ 40) the value of the gap is significantly smaller than the bandgap of c-Si (a PBE estimate[46] of the latter is 0.75 eV, whereas the experimentally derived value is 1.17 eV[46]), is consistent with the conclusion arrived above based on the analysis of the cluster polarizabilities that Si clusters are more metallic than bulk Si.

As a final remark, we note that the extended size range considered in this study is still too small to fully characterize the size-driven evolution in the structural characteristics and

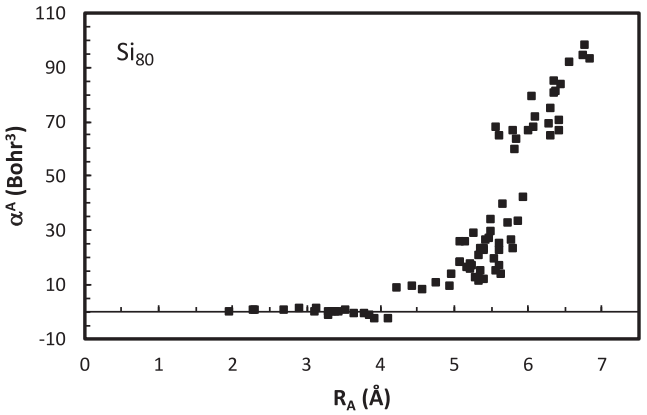

FIG. 3. Values of the site-specific polarizabilities for individual atoms in Si_{80} plotted vs R_A, the distance of the atom from the cluster center of mass.

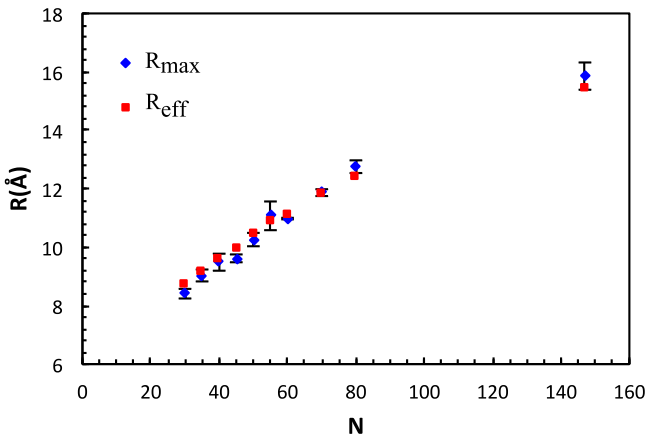

FIG. 4. $R_{eff} = (\alpha^q)^{1/3}$ and R_{max}, the average of the four largest values of R_A, the distance of atom A from the cluster center of mass, for Si_N from $N = 30$ to 147. The error bars indicate the standard deviation in the four values of R_A used to compute R_{max} at each cluster size. See the text for details.

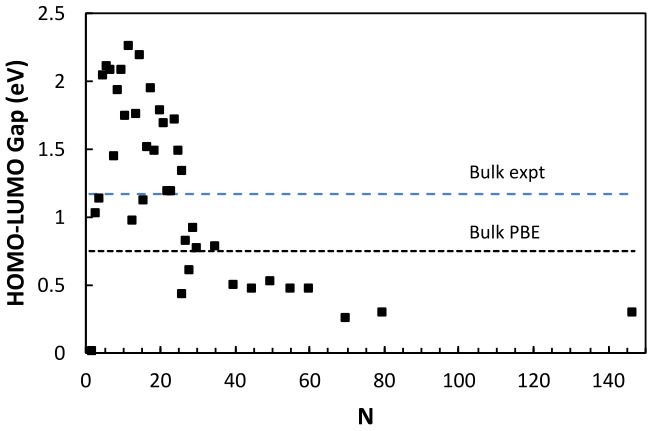

FIG. 5. HOMO-LUMO gap of the lowest-energy Si_N isomers as a function of cluster size N. The value of the bulk crystalline Si bandgap computed within the DFT/PBE framework (0.75 eV) is shown by the dotted line, whereas the experimentally derived value (1.17 eV) is shown by the dashed line. The difference between these two values reflects the well-known underestimation of bandgaps by DFT.

in the response to an external electric field in Si_N that eventually leads to the diamond structure of bulk silicon and its characteristic polarizability. Regarding the structural aspect, it is not known whether the stuffed-fullerene motif will continue to yield the lowest-energy isomers for Si_N larger than those considered here. There have been suggestions that alternative structures with more bulk-like atomic arrangements may become more stable than the stuffed fullerenes at sizes similar to the largest one considered here.[26] As for the polarizability and its dipole and charge transfer components, it is clear that the evolution of $\frac{\alpha^q}{N}$ will involve a downward turn from the linear increase exhibited in Fig. 2 at larger values of N. We also expect that $\frac{\alpha^p}{N}$ will undergo a similar, but upward, turn from its corresponding linear decrease.

IV. SUMMARY

Electric dipole polarizabilities, obtained using DFT-PBE, are presented for low-energy isomers of Si_N over a broad range of sizes up to $N = 147$. The computed effective polarizabilities, α^{eff}, which include the contribution of the permanent electric dipole moment of a cluster, are shown to be in very good agreement with the values derived from experiments for clusters with up to $N = 75$ atoms, the largest size included in the experimental data. The dipole moment contribution to $\frac{\alpha^{eff}}{N}$ is most important for the strongly prolate clusters in the $N = 16$–26 size range; for larger clusters, the $1/N$ factor in the dipole moment dependent term decreases its relative importance. Plots of $\frac{\alpha^p}{N}$ and $\frac{\alpha^q}{N}$—respectively, the local dipole and charge transfer components of $\frac{\alpha}{N}$—versus $N^{-1/3}$ show linear trends for cluster sizes larger than the smallest ones. Extrapolation of these trends to the large size limit ($N^{-1/3} \rightarrow 0$) results in a value of $\frac{\alpha}{N}$ = 30.5 bohrs^3/atom, which is nearly 22% larger than the bulk polarizability of c-Si, 25.06 bohrs^3/atom, obtained from the Clausius-Mossotti relation. It is close to 32.1 bohrs^3/atom, the value that would be a characteristic of a metal with the same volume per atom as c-Si. These results indicate that Si clusters possess a higher degree of metallicity, or metallic-type of response, than bulk Si. The strong electrostatic screening of the cluster interiors further supports this conclusion. Future work should extend these studies to Si clusters of larger sizes and explore the continued size-driven changes in the preferred structural forms and in the way the clusters respond to an external electric field.

SUPPLEMENTARY MATERIAL

See supplementary material for the optimized atomic coordinates and the site-specific polarizability data for all the silicon clusters used in this study.

ACKNOWLEDGMENTS

The authors are grateful to Professor X.-C. Zeng for providing cluster coordinates and to D. Götz and Professor Dr. R. Schäfer for discussions of their experimental data. K.A.J. was supported by the U.S. Department of Energy, Grant No. DE-SC0001330. J.J. was supported by the Office of Basic Energy Sciences, Division of Chemical Sciences, Geosciences and Biosciences, U.S. Department of Energy under Contract No. DE-AC02-06CH11357.

[1] M. F. Jarrold and V. A. Constant, Phys. Rev. Lett. **67**, 2994 (1991).
[2] E. Kaxiras and K. A. Jackson, Phys. Rev. Lett. **71**, 2354 (1993).
[3] B. Liu, Z.-Y. Lu, B. Pan, C.-Z. Wang, and K.-M. Ho, J. Chem. Phys. **109**, 9401 (1998).
[4] K. M. Ho, A. A. Shvartsburg, B. Pan, Z.-Y. Lu, C.-Z. Wang, J. G. Wacker, J. L. Fye, and M. F. Jarrold, Nature **392**, 582 (1998).
[5] L. Mitas, J. C. Grossman, I. Stich, and J. Tobik, Phys. Rev. Lett. **84**, 1479 (2000).
[6] I. Rata, A. A. Shvartsburg, M. Horoi, T. Frauenheim, K. W. M. Siu, and K. A. Jackson, Phys. Rev. Lett. **85**, 546 (2000).
[7] S. Yoo, X. C. Zeng, X. Zhu, and J. Bai, J. Am. Chem. Soc. **125**, 13318 (2003).
[8] Q. Sun, Q. Wang, P. Jena, B. K. Rao, and Y. Kawazoe, Phys. Rev. Lett. **90**, 135503 (2003).
[9] K. Jackson, M. Horoi, I. Chaudhuri, and T. Frauenheim, Phys. Rev. Lett. **93**, 013401 (2004).
[10] W. Hellmann, R. G. Hennig, S. Goedecker, C. J. Umrigar, B. Delley, and T. Lenosky, Phys. Rev. B **75**, 085411 (2007).
[11] R. R. Hudgins, M. Imai, M. F. Jarrold, and P. Dugourd, J. Chem. Phys. **111**, 7865 (1999).
[12] M. F. Jarrold and E. C. Honea, J. Phys. Chem. **95**, 9181 (1995).
[13] S. Yoo, J. J. Zhao, J. L. Wang, and X. C. Zeng, J. Am. Chem. Soc. **126**, 13845 (2004).
[14] J. Zhao, J. Wang, J. Jellinek, S. Yoo, and X. C. Zeng, Eur. Phys. J. D **34**, 35 (2005).
[15] S. Yoo and X. C. Zeng, Angew. Chem., Int. Ed. **44**, 1491 (2005).
[16] S. Yoo and X. C. Zeng, J. Chem. Phys. **124**, 054304 (2006).
[17] S. Yoo, N. Shao, C. Koehler, T. Frauenheim, and X. C. Zeng, J. Chem. Phys. **124**, 164311 (2006).
[18] S. Yoo, N. Shao, and X. C. Zeng, J. Chem. Phys. **128**, 104316 (2008).
[19] S. Yoo, N. Shao, and X. C. Zeng, Phys. Lett. A **373**, 3757 (2009).
[20] R. L. Zhou and B. C. Pan, Phys. Lett. A **368**, 396 (2007).
[21] J. L. Wang, X. L. Zhou, G. H. Wang, and J. J. Zhao, Phys. Rev. B **71**, 113412 (2005).
[22] J. J. Zhao, L. Ma, and B. Wen, J. Phys.: Condens. Matter **19**, 226208 (2007).
[23] J. Wang, J. Zhao, L. Ma, and G. Wang, Eur. Phys. J. D **45**, 289 (2007).
[24] O. Oña, V. E. Bazterra, M. C. Caputo, J. C. Facelli, P. Fuentealba, and M. B. Ferraro, Phys. Rev. A **73**, 053203 (2006).
[25] W. Qin, W.-C. Lu, L.-Z. Zhao, Q.-J. Zang, C.-Z. Wang, and K.-M. Ho, J. Phys.: Condens. Matter **21**, 455501 (2009).
[26] L.-Z. Zhao, W.-S. Su, W.-C. Lu, C.-Z. Wang, and K.-M. Ho, J. Comput. Chem. **32**, 1271 (2011).
[27] I. Vasiliev, S. Ögüt, and J. R. Chelikowsky, Phys. Rev. Lett. **78**, 4805 (1997).
[28] K. Jackson, M. Pederson, C.-Z. Wang, and K.-M. Ho, Phys. Rev. A **59**, 3685 (1999).
[29] K. Deng, J. Yang, and C. T. Chan, Phys. Rev. A **61**, 025201 (2000).

[30]V. E. Bazterra, M. C. Caputo, M. B. Ferraro, and P. Fuentealba, J. Chem. Phys. **117**, 11158 (2002).
[31]C. Pouchan, D. Bégué, and D. Y. Zhang, J. Chem. Phys. **121**, 4628 (2004).
[32]K. A. Jackson, M. Yang, I. Chaudhuri, and T. Frauenheim, Phys. Rev. A **71**, 033205 (2005).
[33]M. Yang, K. A. Jackson, and J. Jellinek, J. Phys. Chem. C **111**, 17952 (2007).
[34]R. Schäfer, S. Schlecht, J. Woenckhaus, and J. A. Becker, Phys. Rev. Lett. **76**, 471 (1996).
[35]D. A. Götz, S. Heiles, R. L. Johnston, and R. Schäfer, J. Chem. Phys. **136**, 186101 (2012).
[36]D. A. Götz, S. Heiles, and R. Schäfer, Eur. Phys. J. D **66**, 293 (2012).
[37]K. Jackson, L. Ma, M. Yang, and J. Jellinek, J. Chem. Phys. **129**, 144309 (2008).
[38]J. P. Perdew, K. Burke, and M. Ernzerhof, Phys. Rev. Lett. **77**, 3865 (1996).
[39]M. R. Pederson and K. A. Jackson, Phys. Rev. B **41**, 7453 (1990).
[40]K. A. Jackson and M. R. Pederson, Phys. Rev. B **42**, 3276 (1990).
[41]D. Porezag and M. R. Pederson, Phys. Rev. A **60**, 2840 (1999).
[42]See http://www-wales.ch.cam.ac.uk/CCD.html for the Cambridge Cluster Database (accessed August 13, 2015).
[43]A. Dal Corso, S. Baroni, and R. Resta, Phys. Rev. B **49**, 5323 (1994).
[44]P. H. Acioli and J. Jellinek, Phys. Rev. Lett. **89**, 213402 (2002).
[45]L. Ma, K. A. Jackson, J. Wang, M. Horoi, and J. Jellinek, Phys. Rev. B **89**, 035429 (2014).
[46]J. Heyd, J. E. Peralta, G. E. Scuseria, and R. L. Martin, J. Chem. Phys. **123**, 174101 (2005).